Gene 851 (2023) 147041

Contents lists available at ScienceDirect

Gene

journal homepage: www.elsevier.com/locate/gene

Gallic acid has an inhibitory effect on skin squamous cell carcinoma and acts on the heat shock protein HSP90AB1

Sabrina Ferreira de Jesus [a], Marcela Gonçalves de Souza [a], Lorena dos Reis Pereira Queiroz [a], Daniela Paola Santos de Paula [a], Angeliny Tamiarana Lima Tabosa [a], Wislene Sarajane Moreira Alves [a], Luiz Henrique da Silveira [a], André Teixeira da Silva Ferreira [b], Ozires José Dutra Martuscelli [c], Lucyana Conceição Farias [d], Alfredo Maurício Batista de-Paula [c], Sérgio Henrique Sousa Santos [e], André Luiz Sena Guimaraes [d,*]

[a] Department of Dentistry, Universidade Estadual de Montes Claros, Minas Gerais, Brazil
[b] Instituto Oswaldo Cruz (IOC), Fiocruz, Rio de Janeiro, Brazil
[c] Hospital Dilson Godinho, Montes Claros, Minas Gerais, Brazil
[d] Departament of Medicine, Universidade Estadual de Montes Claros, Minas Gerais, Brazil
[e] Instituto Federal do Norte de Minas Gerais, Montes Claros Minas Gerais, Brazil

ARTICLE INFO

Edited by: Andre van Wijnen

Keywords:
Bioinformatics
Skin Cancer
Reactive oxygen species

ABSTRACT

Differences in the features of aggressiveness of non-melanoma skin cancer (NMSC) subtypes, between basal cell carcinoma (BCC) and squamous cell carcinoma (SCC) are relevant characteristics. Comparing the characteristics between NMSC subtypes might help identify molecules associated with cancer metastasis and invasion. Considering these facts, the current study aimed to identify a molecular target for inhibiting skin cancer metastasis and invasion.

Proteomic analysis suggested that heat shock protein 90 kDa, alpha, class B member 1 (HSP90AB1), pentaxin (PTX3), caspase-14 (CASP14), S100, actin-1, and profilin were the primary targets related to metastasis and invasion. However, after a differential expression comparison between BCC and SCC, HSP90AB1 was identified as the best target to repress metastasis and invasion. Based on molecular docking results, gallic acid (GA) was selected to inhibit HSP90AB1. A specific Hsp90ab1 siRNA targeting was designed and compared to GA. Interestingly, GA was more efficient in silencing HSP90AB1 than siRNAhsp90ab1. Hence, our data suggest that HSP90AB1 is a crucial biomarker for identifying invasion and metastasis and that its inhibition may be a viable strategy for treating skin cancer.

1. Introduction

In 2020, 1,042,056 new cases of non-melanoma skin cancer (NMSC) was reported to have occured worldwide (Sung et al., 2021). Basal cell carcinoma (BCC) and squamous cell carcinoma (SCC) are the two most common types of NMSC (Fitzmaurice et al., 2019; Ciążyńska et al., 2021). Potentially malignant oral lesions (PMOLs) may undergo spontaneous remission or evolve to become SCC (de Paula Souza et al., 2022). For example, actinic keratosis (AK) is considered a PMOL of the skin (Poswar et al., 2013; de Almeida et al., 2016) because its prognosis is associated with histopathological and molecular findings (Poswar et al., 2013; de Oliveira Poswar et al., 2015).

Abbreviations: NMSC, Non-melanoma skin cancer; BCC, Basal cell carcinoma; SCC, Squamous cell carcinoma; PMOLs, Potentially malignant oral lesions; AK, Actinic keratosis; GA, Gallic acid; NS, Normal skin; TFA, Trifluoroacetic acid; MS, Mass spectrometry; GEO, Gene Expression Omnibus; A431, Epidermoid carcinoma cell line; HaCaT, Skin keratinocyte cell line; MTT, 3-(4,5-dimethylthiazol-2-yl)-2,5-diphenyltetrazolium bromide; DMSO, Dimethyl sulfoxide; PBS, Phosphate-buferid saline; AO, Acridine orange; EB, Ethidium bromide; ROS, Reactive oxygen species; H2DCFDA, Dichlorodihydrofluorescein diacetate; qRT-PCR, Quantitative reverse transcription PCR; cDNA, Complementary deoxyribonucleic acid; RNA, Ribonucleic acid; siRNA, Small interfering RNA ; PTX3, Pentaxin; CASP14, Caspase-14.

* Corresponding author at: Universidade Estadual de Montes Claros. Hospital Universitário Clemente Faria. Laboratório de Pesquisa em Saúde, 562 Av. Cula Mangabeira Santo Expedito. Montes Claros, MG Zip code: 39401-001, Brazil.
E-mail address: andreluizguimaraes@gmail.com (A.L.S. Guimaraes).

https://doi.org/10.1016/j.gene.2022.147041
Received 7 July 2022; Received in revised form 7 November 2022; Accepted 7 November 2022
Available online 12 November 2022

Past studies have suggested pathways related to inhibition of cancer metastasis and invasion (Souza et al., 2010; Souza et al., 2011; de Almeida et al., 2016). Despite recent technological advances, cancer treatment remains a challenge and the clinical benefits remains unclear (Shalhout et al., 2021). Hence, one alternative to avoiding the collateral effects is to identify molecular specific targets (Xavier et al., 2021). Identifying biomarkers associated with invasiveness and metastasis, which can assist in the treatment and prognosis of NMSC, is an auspicious field of research and one that has brought about promising results (Fraga et al., 2012; Cardoso et al., 2019b). One crucial strategy to identifying biomarkers is to compare neoplasia with different prognoses and to select targets according to the behavioral characteristics of the neoplasia (Santos et al., 2021a). Multiple molecular analysis tools, such as proteomics, have emerged for identifying protein-based markers that can become therapeutic targets for the diagnosis, treatment, and monitoring of tumors as well as for understanding tumor biology (Cardoso et al., 2019a). Specifically, when combined with bioinformatics tools (Monção et al., 2020) and additional repository data (Santos et al., 2021b), the validity of proteomics biomarkers has become more robust and reproducible (Santos et al., 2021a; de Paula Souza et al., 2022). Chaperones are proteins related to protein structure/folding, and, consequently, protein function (Schopf et al., 2017). They are also responsible for controlling protein metabolism and degradation (Schopf et al., 2017). In general, the role of chaperones in protein degradation is one of the factors that links chaperones to cancer development and prognosis (Santos et al., 2021b). Recent strategies, such as gene silencing using bioprospecting compounds, have emerged as alternatives to conventional cancer treatment (Guimaraes et al., 2016; Xavier et al., 2021). Therefore, this study aimed to identify a molecular target that can be inhibited to repress skin cancer metastasis and invasion.

2. Materials and Methods

The detailed methodology is presented in the Supplementary Material and Methods.

2.1. Et hical approval

Ethical approval for this study was obtained from the Institutional Ethical Review Board (no. 52769016.9.0000.5146), and informed consent was obtained from all patients who participated in the study.

2.2. Study design

Three different designs were used in this study. In the first part of this study, we performed bioinformatics and clinical analyses. Cell culture was performed as the second step to identify an inhibitor of the selected target. In the third part of the study, the inhibitory activity of gallic acid (GA) was compared with that of siRNA *in vitro*.

2.3. Patients and groups

A total of 16 samples collected between 2010 and 2016 were selected from the Human Biological Bank. The samples were then divided into four groups comprised of frozen samples of AK, BCC, SCC, and normal skin (NS) *(n = 4)* to investigate differences between NMSC subtypes. The control group was comprised of samples from the peritoneal region. The clinical data of the patients are presented in Supplementary Table 1.

2.4. Mass spectrometry analysis

For protein extraction, tissues were first macerated, and then a lysis buffer was added. Briefly, protein extracts were denatured in 1.6 mol/L urea (Sigma-Aldrich, Darmstadt, Germany) followed by reduction with 5 mmol/L dithiothreitol (Sigma-Aldrich) for 25 min at 56 °C, alkylation with 14 mmol/L iodoacetamide (Fluka, Buchs, Switzerland) for 30 min at room temperature in the dark, and trypsin digestion (Promega, Madison, WI, USA) for 16 h at 37 °C (enzyme-to-substrate ratio = 1:50) (Aragão et al., 2012). The digested aliquots were then passed through Poros R2 C8 C18 resin (Invitrogen) with 1 % trifluoroacetic acid (TFA) for desalination. After washing with 0.1 % TFA, the peptides were eluted in 0.1 % TFA with 70 % acetonitrile and dried in a vacuum centrifuge (Cardoso et al., 2019b). Peptide elution was analyzed using mass spectrometry (MS), as described previously (Ma et al., 2003; Cardoso et al., 2019a).

Reversed-phase nano-chromatography coupled with high-resolution nano-electrospray MS was used to identify tripsin digestion. Scaffold software (https://www.proteomesoftware.com) and statistical validation were used to confirm peak protein identification (Ma et al., 2003). The scaffold was then used to probabilistically validate peptide identification using PeptideProphet (Keller et al., 2002) and to derive the corresponding protein probabilities using ProteinProphet (Nesvizhskii et al., 2003; Searle, 2010). Normalized spectral counts were then analyzed using the Green Scaffold software (version 4.0; Proteome Software, Inc., Portland, OR, USA) with a protein threshold higher than 95 % probability to evaluate differentially expressed proteins among groups. A second criterion for analyzing the data obtained using MS was the statistical analysis of a heatmap using the MetaboAnalyst 5.0 software (https://www.metaboanalyst.ca/) (Pang et al., 2022). The data obtained from MS were also analyzed using fold change to compare the expression of proteins between each group studied and NS. The protein level was deemed to be significantly high if its expression had a ratio of 5.0 or higher and a p-value of < 0.05.

2.5. Mass spectrometry validation

Four gene expression profile microarray datasets (GSE45216, GSE45164, GSE53462, and GSE98774) were obtained from the Gene Expression Omnibus (GEO) database (https://www.ncbi.nlm.nih.gov/geo/) (de Paula Souza et al., 2022). Analysis of GSE45216 allowed for the comparison of transcriptomes of 30 SCC and 10 AK tissues while GSE45164 was used to compare the transcriptomes of 10 SCC tissues with three matched NS samples. Analysis of GSE53462 allowed us to evaluate two scenarios: a comparison of the transcriptomes of five SCC samples with 16 BCC samples and a comparison of the transcriptomes of 16 BCC samples with five NS samples. Finally, analysis of the last database, GSE98774, allowed for the comparison of transcriptomes of 18 AK samples with those of 20 NS samples. The clinical data of the patients are provided in Supplementary Table 2. The GEO2R tool (https://www.ncbi.nlm.nih.gov/geo/geo2r/) was used to perform differential expression analyses between individually paired samples from each database (de Paula Souza et al., 2022). The Benjamini and Hochberg false discovery rate method was applied to correct the occurrence of false-positive results. A logFC (fold change) value ≥ 1 was considered the cutoff criterion (Sun et al., 2017; Pereira et al., 2019). The tissue expression of selected genes in NS, BCC, and SCC is available in the Human Protein Atlas (https://www.proteinatlas.org/) (Uhlen et al., 2017).

2.6. Molecular docking

The 3D chemical structures of GA and the HSP90AB1 protein (PDB ID: 3 NMQ) (Wang et al., 2018) were obtained from PubChem (https://pubchem.ncbi.nlm.nih.gov/) and the RCSB Protein Data Bank (https://www.rcsb.org/), respectively. The UCSF Chimera software (version 1.13) was used to prepare the two molecules for molecular coupling (Qawoogha and Shahiwala, 2020). The Achilles Blind Docking online server (https://bio-hpc.eu/software/blind-docking-server/) was used to predict the types of bonds and to calculate the free bond energy between the protein and compound used. This server uses the “blind coupling” approach, as the protein-binding site has not been specified (Sánchez-Linares et al., 2012).

2.7. Cell culture

A431 and HaCaT cells were kindly given to us by Dr. Lídia Maria de Andrade (Nanobiomedical Research Group, Department of Physics, ICEx/Federal University of Minas Gerais) and were cultured as described before (Tabosa et al., 2022). The A431 cell line was derived from SCC and was used for *in vitro* testing (Tiwari et al., 2017). The cells were grown in Dulbecco's modified Eagle's medium (Gibco, Billings, MT, USA) supplemented with 10 % fetal bovine serum (Gibco), 400 ng/mL hydrocortisone, and an antibiotic/antimycotic solution (Invitrogen, Carlsbad, CA, USA) and were incubated at 37 °C with 5 % CO_2 in a humidified air atmosphere. The treatment used in the tests included GA 3,4,5-trihydroxy benzoic acid 97.5 %–102.5 % (titration)(Sigma, St. Louis, MO, USA).

2.8. Phenotypic assays: MTT, wound scratch, cell death, and reactive oxygen species.

The 3-(4,5-dimethylthiazol-2-yl)-2,5-diphenyltetrazolium bromide (MTT) test was performed to determine the concentration of GA. Briefly, A431 and HaCaT cells were plated at a density of 3×10^3 cells/well and treated with GA at various concentrations. GA was dissolved in ethanol, and seven groups were used: control, vehicle, 1, 5, 10, 15, and 20 μg/mL of GA. After 24 h, cells were washed with 1X PBS. After washing, cells were subjected to the MTT reagent (Thermo Fisher Scientific, Waltham, MA, USA), which was solubilized with dimethyl sulfoxide (DMSO) (Sigma-Aldrich, St. Louis, MO, USA) and turned to a blue/purple color. Measurements were performed using ELISA equipment at an absorbance value of 540 nm, and the results were obtained from triplicate experiments. The importance of each group was statistically analyzed (Guimaraes et al., 2016), and an MTT assay was performed using the color intensity of formazan crystals. All group color intensity values were assessed using the ImageJ software (da Rocha et al., 2019). Cell viability was evaluated using the MTT assay, followed by an analysis of IC_{50} values in the A431 and HaCaT cells. The results of the MTT assays were assessed as A431, and HaCaT cells were used in *in vitro* assays and received the following groups: control, vehicle, and 10 μg/mL GA. All experiments were performed in triplicates. Briefly, for the wound scratch assay, a scratch was made with a sterile pipette tip (2–20 μL) in a confluent cell layer, and this was followed by washing twice with PBS and without or with the addition of 10 μg/mL GA in serum-free medium (Locatelli et al., 2013). Wells were photographed at the beginning of the experiment and 24 h after treatment. ImageJ was used for the analysis (Guimaraes et al., 2016).

To analyze the ratio of dead cells to total cells, all groups were stained with a solution containing 1,000 μg/mL acridine orange (LA; Sigma) and 100 μg/mL ethidium bromide (BE; Sigma). An FSX100 microscope (Olympus, Center Valley, PA, USA) was used for image analysis (Guimaraes et al., 2016). To measure the levels of reactive oxygen species (ROS), cells were incubated with 10 μmol/L dichlorodihydrofluorescein diacetate (H2DCFDA; Invitrogen) for 30 min at 37 °C, washed twice with 1X PBS, and immediately photographed under a fluorescence microscope (Olympus), and then quantified using ImageJ (Bander et al., 2019).

2.9. qRT-PCR and immunocytochemical analysis

Per the manufacturer's instructions, RNA was isolated using the TRIzol reagent (Thermo Fisher Scientific). For qRT-PCR, 66 ng of cDNA was added to SYBR Green reagent (Life Technologies, Carlsbad, CA, USA) with Hsp90ab1-specific primers (forward: 5- CAAGGGAAAAGCCAGAAGATAGCA −3; reverse: 5- CCAGGCACTTCGGGACAACTC −3) (De Spiegelaere et al., 2015; Nikishin et al., 2018) (Integrated DNA Technologies, Inc., San Diego, CA, USA). Amplification was performed using a QuantStudio 6 qRT-PCR system (Life Technologies). All reactions were performed in triplicate, and β-actin (forward primer: 5-AGGCACCAGGGCGTGAT −3; reverse primer: 5- GCCCACATAGGAATCCTTCTGAC −3) (Bravo-Calderon et al., 2020) was used as an endogenous control for the normalization of target gene expression. The analysis of the qRT-PCR data was performed using the $2^{-\Delta\Delta Ct}$ method. For immunocytochemical analysis, cells were seeded on glass coverslips and synchronized for 24 h by serum starvation, and then GA was added to the culture medium. The following primary mouse monoclonal antibody was used: anti-HSP90AB (F-8)(1:100, sc-13119; Santa Cruz Biotechnology, Inc., Dallas, TX, USA). Briefly, the samples were incubated with the monoclonal antibody for 18 h at 4 °C. Endogenous peroxidase was blocked by incubating with 0.3 % H_2O_2 in Milli-Q water for 30 min. Signals were developed using 3,3'-diaminobenzidine tetrahydrochloride for 3 min, followed by counterstaining with Mayer's hematoxylin for 1 min. Positive and negative controls were used for all reactions. The slides were photographed under an FSX100 bright-field microscope (Olympus, Center Valley, PA, USA) at 40 × magnification. Immunocytochemical analyses of the investigated antigens were performed by determining the percentage of positively stained cells in all counted fields. Cytoplasmic staining of HSP90AB1 was positive (Guimaraes et al., 2016).

2.10. siRNA-mediated downregulation of HSP90AB1 and the effect of gallic acid

First, A431 cells were transfected with siRNA directed against HSP90AB1 using the Lipofectamine RNAiMAX transfection reagent (Life Technologies, Carlsbad, CA, USA). siRNA (s7000 and s7001) were purchased from Life Technologies, and the BLOCK-iT ™ Alexa Fluor® Red Fluorescent Control siRNA (Life Technologies, Carlsbad, CA, USA) was used as both a transfection control and a scramble control according to the manufacturer's instructions (Life Technologies, Carlsbad, CA, USA) (HaDuong et al., 2015). GA was used as an inhibitor of HSP90AB1, for comparison with the inhibitory activities of the s7000 and s7001 siRNAs. Wound scratch assays, cell death assays, and immunocytochemical analysis were performed in triplicate for each group.

2.11. Statistical analysis

All analyses were performed using SPSS Inc. Released 2009. PASW Statistics for Windows, version 18.0 (Chicago: SPSS Inc., USA) and GraphPad Prism (version 5.0; GraphPad Software, Inc., San Diego, CA, USA). Kolmogorov-Smirnov and Shapiro-Wilk tests were used to assess data distribution. Because the samples showed a normal distribution, a one-way analysis of variance (ANOVA) was performed, and Tukey's test followed this. All data are presented as mean ± standard deviation. Statistical significance was set at $p < 0.05$.

3. Results

3.1. HSP90AB1 is the target associated with the aggressive behavior of SCC

MS analysis was performed to trace the protein profiles of AK, BCC, SCC, and NS samples. In total, 29 proteins with a 95 % detection rate were selected. Heatmap analysis revealed that the primary protein candidates were associated with a high level of invasiveness and aggressiveness in SCC (Fig. 1A). Fold-change analysis was used to compare the expression of proteins between each case group and the NS group. A protein level was considered significantly high if it had a score ratio of 5.0 or higher and a *p*-value of < 0.05 (Supplementary Table 3). The proteins included in the fold-change analysis were as follows: heat shock protein 90 kDa, alpha, class B member 1 (HSP90AB1), pentaxin (PTX3), caspase-14 (CASP14), S100, actin-1, and profilin (Fig. 1A).

A total of 127 samples were included in this analysis and comprised 45 SCC, 16 BCC, 28 AK, and 38 NS samples. Each dataset was subjected to differential expression analysis using GEO2R (Supplementary

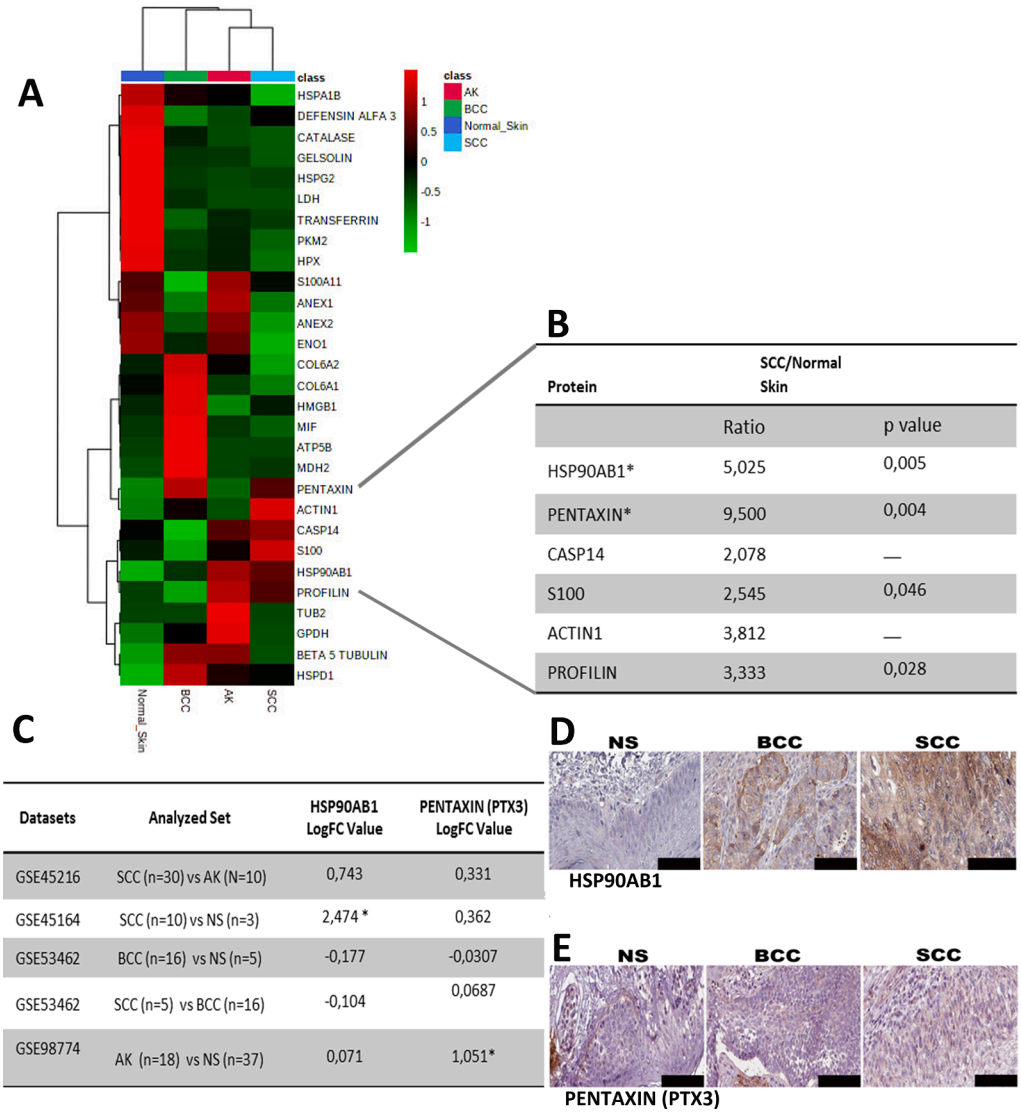

Fig. 1. (A) Statistical analysis of heatmap. 29 proteins with 95 % detection were selected. The main protein candidates to be associated with higher invasiveness and agressivess of SCC (B) The main candidate proteins to be associated with greater invasiveness and aggressiveness of the SCC had a fold-change value ratio $\geq$ 5.0 and p-value $<$ 0.05. *HSP90AB1 and PENTAXIN have been selected. (C) Differential expression Panel (HSP90AB1 and PENTAXIN (PTX3) validation). Diferential expression in GEO. NOTE: logFC, logarithmic fold change. SCC – skin squamouss cell cancer, AK- actinic keratosis, BCC- Basocelular cell cancer, NS- normal skin./ * To be considered as significant diferential expression value, logFC 1 was set as the cuttoff criterion. (D) HSP90AB1 imunohistochemistry from NS, BCC, and SCC tissues. (E) PENTAXIN (PTX3) imunohistochemistry from NS, BCC and SCC tissues (images from Protein Atlas Database).

Table 3). After an active search, the HSP90AB1 and PTX3 genes were found to be expressed in all the datasets analyzed in this study (Fig. 1C). Notably, the HSP90AB1 and PTX3 proteins showed a higher ratio than that of other proteins and a significant *p*-value when comparing SCC to NS (Fig. 1B).

Cutoff criteria were applied to interpret the differential expression analysis results. Thus, it was possible to infer that the differential expression of HSP90AB1 was significant only when SCC and NS were compared (Fig. 1C). No significant differential expression was observed between SCC and AK, SCC and BCC, AK and NT, or BCC and NT (Fig. 1C). Thus, the elevation of HSP90AB1 was exclusively associated with SCC (Fig. 1C). Interestingly, neither HSP90AB1 nor PTX3 dysregulation was associated with BCC (Fig. 1C). Moreover, no significant differences in expression were observed for either HSP90AB1or PTX3 when comparing SCC to AK, BCC to NS, or SCC to BCC (Fig. 1C).

Fig. 1D shows the representative immunohistochemical staining characteristics of HSP90AB1 and PTX3 in healthy individuals and patients with cancer. Immunohistochemistry demonstrated an association between HSP90AB1 and SCC (Fig. 1D), whereas the expression of PTX3 was low. Notably, the protein atlas did not contain AK samples. A comparison of protein expression suggests that HSP90AB1 is a molecular marker of malignancy.

3.2. GA binds to the HSP90AB1 protein

In the current study, molecular docking was used to test whether GA affected the HSP90AB1 protein. The docking results showed that the GA molecule binds to several amino acid residues of HSP90AB1, resulting in 13 linkage clusters (Fig. 2A, I-II). The GA high-energy clusters are numbered 1 and 2 (−6.1 kcal/mol and − 5.3 kcal/mol, Fig. 2A, III-IV, respectively). In the first cluster, a hydrogen bond was present between the amino acid residue Trp162 and the –COOH group, a hydrophobic interaction was present between Leu107 and the –CH group, and π stacking interactions were present between the aromatic ring of GA and the Phe138 and Trp162 residues (Fig. 2A, V). In the second cluster, hydrogen bonds were present between the amino acid residues Val172, Glu18, and Glu14 and the –OH group; hydrophobic interactions were present between the Lys100, Tyr160, and Ala174 residues and the –CH groups, and a salt bridge was present between Lys100 and the –COOH group (Fig. 2A, VI). These *in silico* results indicated that GA interacts with and binds to HSP90AB1 and may exhibit biological activity on the studied protein.

3.3. GA dose–response curve in different cell lines

An MTT test was performed to build a GA dose–response curve (Supplementary Material 1, Fig. 1A–1B). The IC_{50} values of aggressive

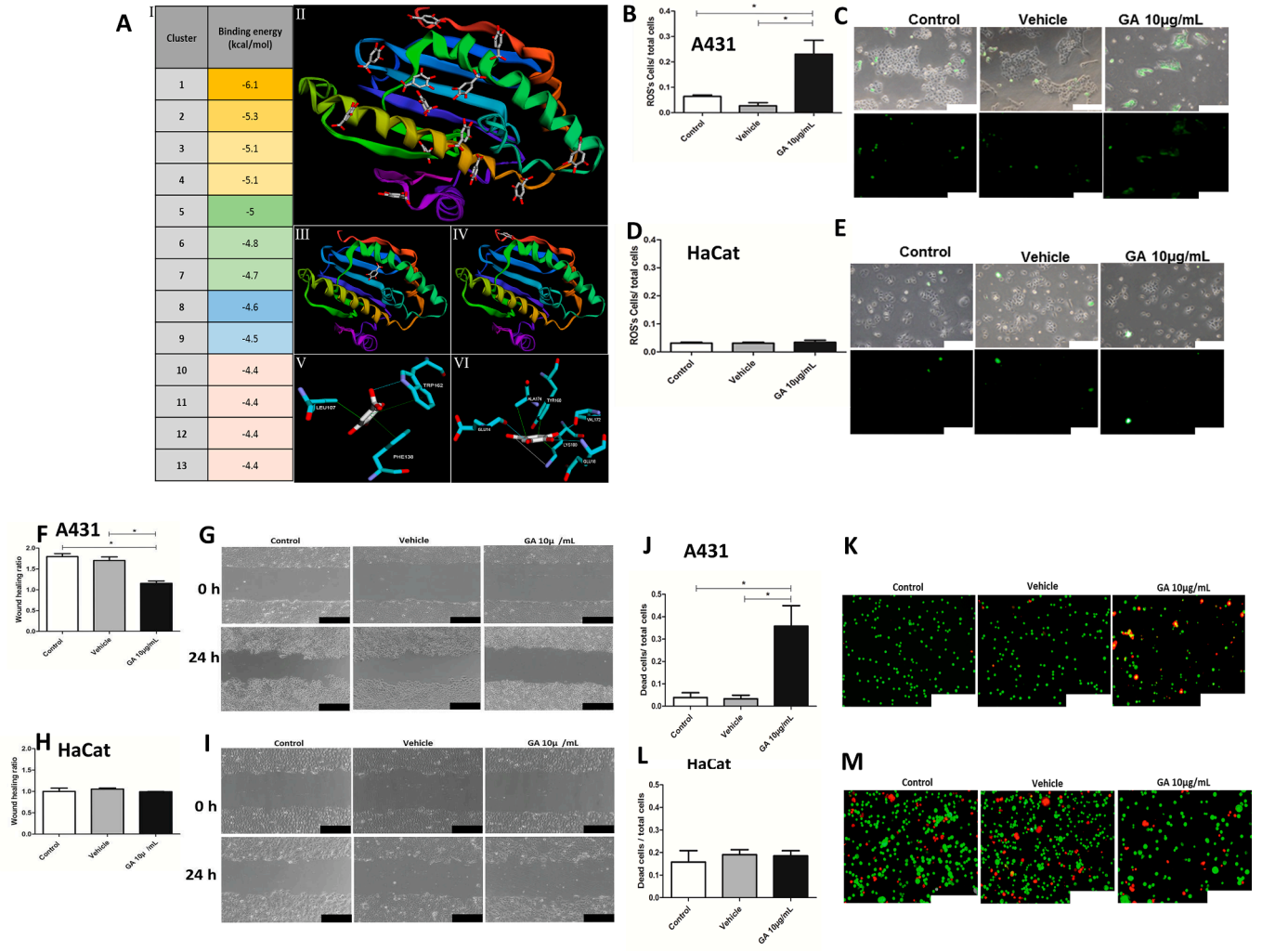

Fig. 2. (A) Molecular docking between gallic acid (GA) and HSP90AB1 protein. (I) The table shows the connection energy values for each of the clusters identified. (II) Visualization of the results of the main clusters. (III) Overview of the GA anchored to HSP90AB1, with a free connection energy of −6.1 kcal/mol. (IV) Overview of the AG anchored to HSP90AB1, with free connection energy of −5.3 kcal/mol. (V and VI) Protein - ligand interactions. * Fluorescent green line: hydrophobic interactions; blue line: hydrogen bonds; white line: salt bridge; dark green line: pi stacking. (B-C) Graphs and microscopic images showing the reactive oxygen species (ROS) rate on cell lines of the skin carcinoma treated with GA at 10 µg/mL. There was an increase in the rate of ROS in skin carcinoma cells line; (D-E) There was no difference in ROS expression between groups of the keratinocyte cell lines. (F-G) After 24 h, there was a significant inhibition of the migration of the skin carcinoma cell lines treated with GA 10 µg/mL; (H-I) In keratinocyte cells, there was no significant inhibition of the migration of cells treated with GA 10 µg/mL; (J-M) Cell death assay performed on skin carcinoma and keratinocyte cell lines treated with GA 10 µg/mL using acridine orange and ethidium bromide; dead skin carcinoma cells in the group treated with GA was significantly higher. In contrast, in keratinocyte cells, there was no significant decrease in the number of dead cells. The scale of 100 µm. *Statistical significance accepted at $p < 0.05$. (For interpretation of the references to color in this figure legend, the reader is referred to the web version of this article.)

cells (A431) and immortalized keratinocytes (HaCaT) were found to be different (7.15 and 13.29, respectively) (Supplementary Material 1, Figs. 2 and 3). Therefore, a 10 µg/mL concentration was chosen to be more effective for A431 cells than for HaCaT cells.

3.4. GA selectively increases the level of ROS in aggressive cells

In skin carcinoma cells, the rate of ROS generation was much higher in cells treated with 10 µg/mL of GA than in the control and vehicle groups (Fig. 2B and 2C). By contrast, no significant differences in the rate of ROS generation were detected in GA-treated keratinocytes (Fig. 2D and 2E).

3.5. GA reduces the migration of SCC cells

A cell migration assay was performed to assess the effects of 10 µg/mL of GA on cell cycle inhibition in both skin carcinoma and keratinocytes. After 24 h, the migration of skin carcinoma cells treated with GA was significantly inhibited compared to control and vehicle-treated cells (Fig. 2F and 2G). However, no significant inhibition was observed in GA-treated keratinocytes (Fig. 2H and 2I). These results indicate that GA induces an anti-migratory effect in the SCC cell line.

3.6. GA causes skin carcinoma cell death

Various assays using ethidium bromide and acridine orange were performed to assess whether GA (10 µg/mL) induced cell death. The percentage of dead skin carcinoma cells in the GA-treated group was significantly higher than in the control and vehicle groups (Fig. 2J and 2 K). By contrast, keratinocytes treated with GA showed no significant increase in dead cells compared to cells in the control and vehicle groups (Fig. 2L and 2 M). These results demonstrate that GA causes the death of skin carcinoma cells but not keratinocytes.

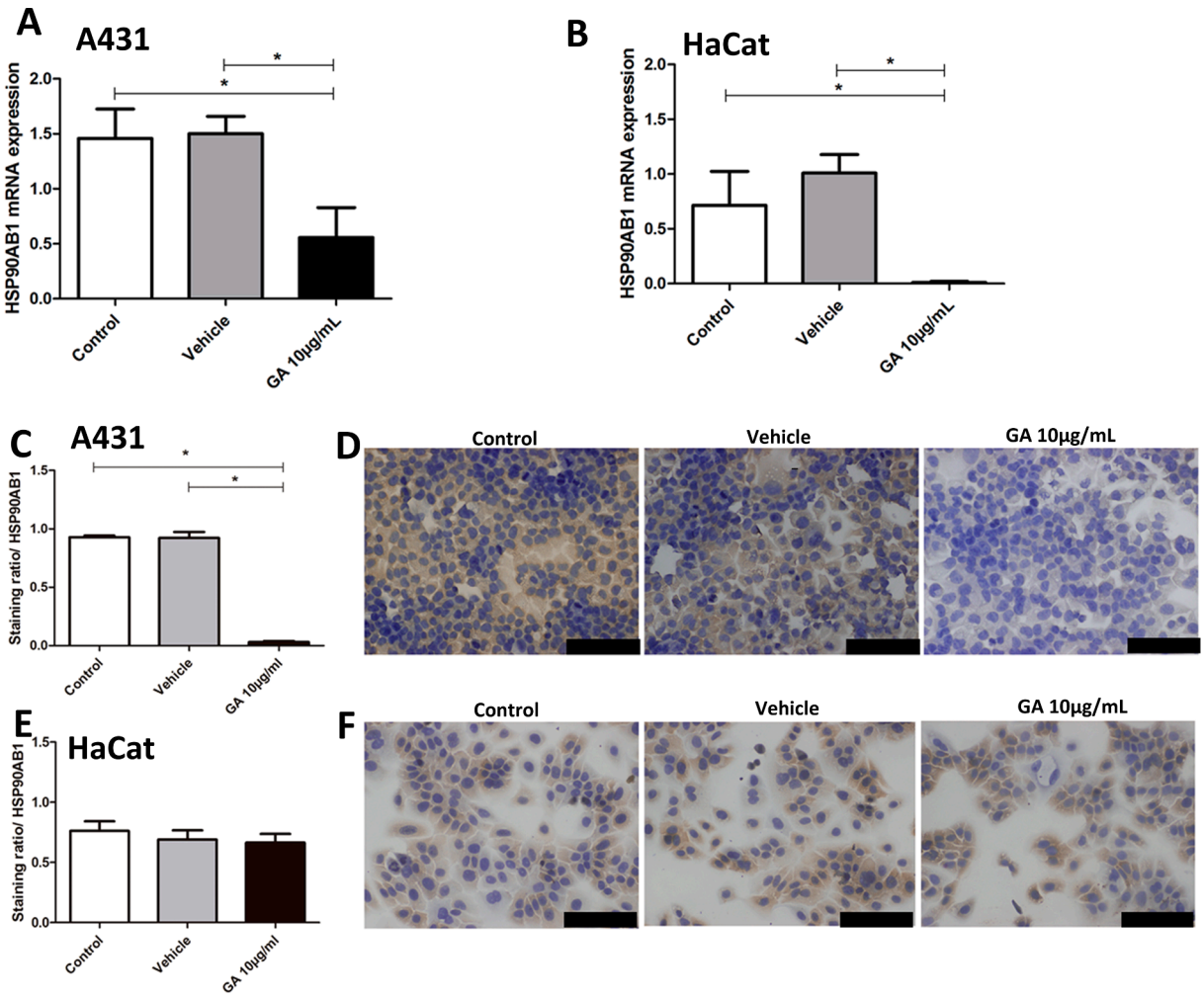

Fig. 3. (A) Graphs of Hsp90ab1 mRNA expression on skin carcinoma and keratinocyte cell lines treated with GA at 10 μg/mL. In the skin carcinoma cell lines, GA decreased the expression of Hsp90ab1; (B) In the keratinocyte cell lines, GA also decreased the gene expression of Hsp90ab1. (C-D) HSP90AB1 protein expression by immunocytochemistry on skin carcinoma cell lines treated with GA 10 μg/mL. In the skin carcinoma cell lines, the expression of HSP90AB1 was decreased; (E-F) In the keratinocyte cell lines, GA 10 μg/mL showed no decreased protein expression. The scale of 100 μm. *Statistical significance accepted at $p < 0.05$.

3.7. GA reduces HSP90AB1 levels in skin carcinoma cells

qRT-PCR was performed to assess whether GA (10 μg/mL) affected Hsp90ab1 gene expression. The levels of Hsp90ab1 mRNA in skin carcinoma cells in the GA-treated group were significantly lower than those in the control and vehicle groups (Fig. 3A). In addition, Hsp90ab1 mRNA expression in GA-treated keratinocytes was significantly lower than in the control and vehicle groups (Fig. 3B). These results indicate that GA affects the expression of Hsp90ab1.

Immunocytochemical analysis was performed to assess whether GA (10 μg/mL) affected HSP90AB1 protein expression. The levels of HSP90AB1 protein in skin carcinoma cells in the GA-treated group were significantly lower than those in the control and vehicle groups (Fig. 3C and 3D). However, HSP90AB1 protein expression levels in GA-treated keratinocytes were insignificant compared to those in the control and vehicle groups (Fig. 3E and 3F). These results indicate that GA selectively affects the expression of HSP90AB1 in skin carcinoma cells.

3.8. Comparison between GA and specific inhibition

Cell death and migration assays showed that siRNA targeting Hsp90ab1 (siRNAhsp90ab1) did not induce the death nor inhibit the migration of skin carcinoma cells (Fig. 4A–4E). However, it was found that GA promoted a decrease in migration and an increase in the death of skin carcinoma cells. The immunocytochemical analysis also revealed that GA and siRNAhsp90ab1 decreased the expression of the HSP90AB1 protein. However, GA was more efficient in silencing HSP90AB1 than siRNAhsp90ab1 (Fig. 4F and 4G). Thus, it can be concluded that GA is more efficient than siRNA in blocking HSP90AB1 expression.

4. Discussion

Given their therapeutic and preventive effects on various diseases associated with oxidative stress, plant phenolic compounds have increasingly attracted the attention of researchers seeking new forms of cancer treatment (Xavier et al., 2021). For example, GA efficiently inhibits bladder cancer cells' migration, invasion, and proliferation (Liao et al., 2018; Santos et al., 2018) and induces apoptosis in lymphoblastic leukemia cells (Sourani et al., 2016). In addition, GA has also been shown to inhibit the migration, proliferation, and invasion of oral SCC (Guimaraes et al., 2016).

Invasive cancer is characterized by the ability of cancer cells to invade other layers of the original organ, thereby gaining the ability to disseminate to other body organs (Domingos et al., 2017). Therefore, cell invasion and migration are critical cellular mechanisms required to initiate this process. Recently, metastatic SCC has become an increasingly common and challenging entity that necessitates the exploration of new treatment options (Santos et al., 2021a; Tabosa et al., 2022).

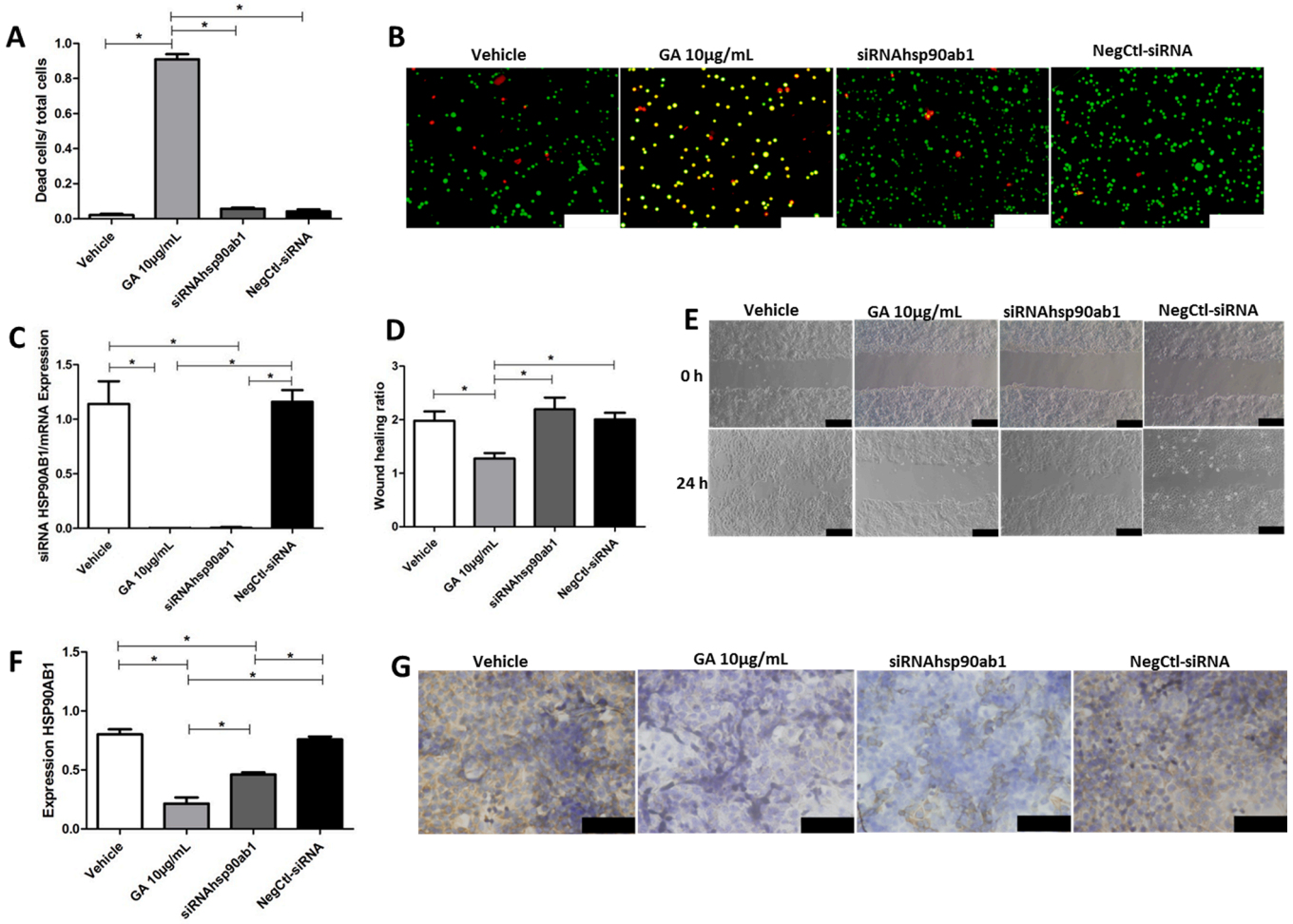

Fig. 4. siRNA-mediated downregulation of Hsp90ab1 and effect of GA in skin carcinoma cell lines. The silencing of Hsp90ab1 was performed and GA had an inhibitory effect on Hsp90ab1. (A-B) Cell death assay performed on skin carcinoma cell lines treated with GA 10 µg/mL and siRNAhsp90ab1. GA promoted the increased death of skin carcinoma cells. The cell death and migration assays show that the siRNAhsp90ab1 group did not cause death or inhibit the migration of skin carcinoma cells (C) siRNAhsp90ab1 and effect of the GA downregulation of mRNA Hsp90ab1. (D-E) GA promoted the decrease in migration of the skin carcinoma cells; (F-G) Immunocytochemistry analysis showed that GA decreased the expression of the HSP90AB1 protein. GA is more efficient in silencing HSP90AB1 than inducing silencing. The scale of 100 µm. *Statistical significance accepted at $p < 0.05$.

In this study, we analyzed the proteomic profiles of different types of NMSC (AK, BCC, and SCC). Among the neoplasms analyzed, SCC is the most malignant (Rosenberg et al., 2019). Therefore, it is necessary to focus on identifying differentially expressed genes in NMSC to understand carcinogenesis better (de Paula Souza et al., 2022). The data from the current study suggests that HSP90AB1 dysregulation is associated with SCC. Therefore, various gene expression datasets were compared to validate the characterization and expression of the Hsp90ab1 target gene in SCC, AK, BCC, and NS. We used GEO2R to identify the differentially expressed genes in each dataset, allowing us to place 3,598 highly expressed genes and 3,345 downregulated genes. After an active search, the Hsp90ab1 gene was found in all datasets analyzed. These findings may support the association of HSP90AB1 with the process of carcinogenesis and progression of premalignant lesions in SCC.

In this study, we evaluated the potential of GA to inhibit HSP90AB1, and the results demonstrated that GA not only reduced HSP90AB1 levels but also had inhibitory effects on the migration of cancer cells. GA can act in different ways to inhibit cell migration and proliferation and regulate genes involved in metastasis, angiogenesis, cell cycle progression, and apoptosis of cancer cells (Guimaraes et al., 2016; Santos et al., 2018). GA also decreases cell viability by arresting the cell cycle in the G1 phase (Lee et al., 2017). In this study, we measured the level of ROS in skin carcinoma cells and found that it was higher in the GA-treated cells than in the control and vehicle groups. According to the literature, GA has been reported to have antioxidant effects. GA has increased ROS generation in cervical cancer cells (Park, 2017). It also appears essential in inducing cell apoptosis through ROS generation (Hsu et al., 2016). Here, we showed increased ROS levels and death in GA-treated cells. Cell death may be due to the higher ROS production induced by GA, as shown in another study (Tabosa et al., 2022). In this study, we not only analyzed cell viability using an MTT assay but also analyzed the IC_{50} in A431 and HaCaT cells. The results showed that the cytotoxic effect of GA on skin carcinoma cells was more significant than that on skin keratinocytes. A previous study also showed differences between the IC_{50} values of HaCaT and A431 cells, which corroborates with previous study (Tabosa et al., 2022).

According to the literature, HSP90 is highly expressed in several tumors. HSP90 is a protein consisting of several molecules responsible for tumor progression and decreased survival, such as hypoxia-inducible factor 1-alpha (HIF-1a) (Fraga et al., 2012; Santos et al., 2021a). In this study, proteomic analysis revealed that high levels of HSP90AB1 were associated with SCC (Bander et al., 2019). In gastric cancer, the increased expression of HSP90AB1 is essential in promoting cell proliferation and metastasis. When this protein is silenced, cell proliferation, migration, and invasion are inhibited (Zhou et al., 2019). It was also found that in metastatic melanoma, HSP90AB1 expression is associated

with disease progression, reduced survival, an increased likelihood of ulceration and increased mitotic rate, and an increased tumor thickness (Metri et al., 2017). In this study, we showed that GA, like siRNAhsp90ab1, could decrease the mRNA and protein expression of HSP90AB1 in skin carcinoma cells. However, while GA could induce cell death and impair migration, silencing Hsp90ab1 with siRNAhsp90ab1 alone was insufficient to cause these effects.

Hence, developing new therapeutic modalities using HSP90AB1 inhibitors can pave the way for treating various pathologies involving this protein (Chong et al., 2019; Milanesi et al., 2019). Natural compounds have been widely studied because of their therapeutic actions (Xavier et al., 2021). For example, the essential oil of *Cymbopogon flexuosus* is a potent inhibitor of Hsp90, whereas withaferin A, a plant-derived ester, has been found to inhibit Hsp90 in B-cell lymphoma (McKenna et al., 2015; Gaonkar et al., 2018).

In this study, cells treated with GA showed decreased migration, increased apoptosis, and higher ROS production. Furthermore, GA reduced HSP90AB1 expression. In addition to GA reducing the expression of HSP90AB1 mRNA in cancer cells, GA also reduced HSP90AB1 protein expression. However, interestingly, the level of HSP90AB1 protein was not reduced in keratinocytes. Therefore, it can be inferred from the ROS and cell death assay results that GA at a concentration of 10 μg/mL does not affect keratinocytes. It is important to emphasize that another cancer cell line was not tested in this study because a research group has already shown that 10 μg/mL of GA reduces migration and proliferation and induces cell death in cancer cells (Guimaraes et al., 2016).

In summary, treatment of skin carcinoma cells with GA at a concentration of 10 μg/mL resulted in cell death, increased ROS generation, and reduced expression of HSP90AB1 mRNA and protein. However, 10 μg/mL GA did not cause cell death nor influence the ROS generation rate in keratinocyte cells. Therefore, it can be concluded that GA at a concentration of 10 μg/mL has an inhibitory effect on skin SCC and the HSP90AB1 biomarker but does not impair the function of keratinocytes. Thus, the deregulation of HSP90AB1 may be related to carcinogenesis and can be used as a molecular marker to predict the progression of premalignant lesions in SCC.

Declaration of Competing Interest

The authors declare that they have no known competing financial interests or personal relationships that could have appeared to influence the work reported in this paper.

Data availability

The authors do not have permission to share data.

Acknowledgments

We would like to thank Dra. Lídia Maria de Andrade for donating A431 and HaCat cells used in this study. We also thank Fundação Oswaldo Cruz Vice (FioCruz)- Rede de Plataformas Tecnológicas - Manguinhos /Rio de Janeiro- Brazil for MS analysis. This study was supported by grants from the Conselho Nacional de Desenvolvimento Científico e Tecnológico (CNPq), Coordenação de Aperfeiçoamento de Pessoal de Nível Superior (CAPES), and the Fundação de Amparo à Pesquisa do Estado de Minas Gerais (FAPEMIG). Dr. Guimarães, Dr. Santos, and Dr. de Paula are research fellows at CNPq.

Appendix A. Supplementary data

Supplementary data to this article can be found online at https://doi.org/10.1016/j.gene.2022.147041.

References

Aragão, A.Z., Belloni, M., Simabuco, F.M., Zanetti, M.R., Yokoo, S., Domingues, R.R., Kawahara, R., Pauletti, B.A., Gonçalves, A., Agostini, M., Graner, E., Coletta, R.D., Fox, J.W., Paes Leme, A.F., 2012. Novel processed form of syndecan-1 shed from SCC-9 cells plays a role in cell migration. PLoS One 7, e43521.

Bander, T.S., Nehal, K.S., Lee, E.H., 2019. Cutaneous Squamous Cell Carcinoma: Updates in Staging and Management. Dermatol Clin 37, 241–251.

Bravo-Calderon, D.M., Assao, A., Garcia, N.G., Coutinho-Camillo, C.M., Roffe, M., Germano, J.N., Oliveira, D.T., 2020. Beta adrenergic receptor activation inhibits oral cancer migration and invasiveness. Arch Oral Biol 118, 104865.

Cardoso, C.M., de Jesus, S.F., de Souza, M.G., Queiroz, L., Santos, E.M., Dos Santos, E.P., Oliveira, L.P., Cordeiro Santos, C.K., Santos, S.H.S., de Paula, A.M.B., Farias, L.C., Guimaraes, A.L.S., 2019a. High levels of ANXA2 are characteristic of malignant salivary gland tumors. J Oral Pathol Med 48, 929–934.

Cardoso, C.M., de Jesus, S.F., de Souza, M.G., Santos, E.M., Santos, C.K.C., Silveira, C.M., Santos, S.H.S., de Paula, A.M.B., Farias, L.C., Guimarães, A.L.S., 2019b. Is HIF1-a deregulated in malignant salivary neoplasms? Gene 701, 41–45.

Chong, K.Y., Kang, M., Garofalo, F., Ueno, D., Liang, H., Cady, S., Madarikan, O., Pitruzzello, N., Tsai, C.H., Hartwich, T.M.P., Shuch, B.M., Yang-Hartwich, Y., 2019. Inhibition of Heat Shock Protein 90 suppresses TWIST1 Transcription. Mol Pharmacol 96, 168–179.

Ciążyńska, M., Kamińska-Winciorek, G., Lange, D., Lewandowski, B., Reich, A., Sławińska, M., Pabianek, M., Szczepaniak, K., Hankiewicz, A., Ułańska, M., Morawiec, J., Błasińska-Morawiec, M., Morawiec, Z., Piekarski, J., Nejc, D., Brodowski, R., Zaryczańska, A., Sobjanek, M., Nowicki, R.J., Owczarek, W., Słowińska, M., Wróbel, K., Bieniek, A., Woźniacka, A., Skibińska, M., Narbutt, J., Niemczyk, W., Ciążyński, K., Lesiak, A., 2021. The incidence and clinical analysis of non-melanoma skin cancer. Scientific Reports 11, 4337.

da Rocha, R.G., Santos, E.M.S., Santos, E.M., Gomes, E.S.B., Ramos, G.V., Aguiar, K.M., Goncalves, B.R., Santos, S.H.S., De Paula, A.M.B., Guimaraes, A.L.S., Farias, L.C., 2019. Leptin impairs the therapeutic effect of ionizing radiation in oral squamous cell carcinoma cells. J Oral Pathol Med 48, 17–23.

de Almeida, C.M., de Jesus, S.F., Poswar Fde, O., Gomes, E.S., Fraga, C.A., Farias, L.C., Santos, S.H., Feltenberger, J.D., de Paula, A.M., Guimarães, A.L., 2016. Increasing demonstration of angiogenic markers in skin neoplastic lesions. Pathol Res Pract 212, 101–105.

de Oliveira Poswar, F., de Carvalho Fraga, C.A., Gomes, E.S., Farias, L.C., Souza, L.W., Santos, S.H., Gomez, R.S., de-Paula, A.M., Guimarães, A.L., 2015. Protein expression of MMP-2 and MT1-MMP in actinic keratosis, squamous cell carcinoma of the skin, and basal cell carcinoma. Int J Surg Pathol 23, 20–25.

de Paula Souza, D.P.S., Dos Reis Pereira Queiroz, L., de Souza, M.G., de Jesus, S.F., Gomes, E.S.B., Vitorino, R.T., Santos, S.H.S., Farias, L.C., de Paula, A.M.B., D'Angelo, M., de Carvalho Fraga, C.A. and Guimaraes, A.L.S., 2022. Identification of potential biomarkers and survival analysis for oral squamous cell carcinoma: A transcriptomic study. Oral Dis.

De Spiegelaere, W., Dern-Wieloch, J., Weigel, R., Schumacher, V., Schorle, H., Nettersheim, D., Bergmann, M., Brehm, R., Kliesch, S., Vandekerckhove, L., Fink, C., 2015. Reference gene validation for RT-qPCR, a note on different available software packages. PLoS One 10, e0122515.

Domingos, P.L.B., Souza, M.G., Guimaraes, T.A., Santos, E.S., Farias, L.C., de Carvalho Fraga, C.A., Jones, K.M., Santos, S.H.S., de Paula, A.M.B., Guimaraes, A.L.S., 2017. Hypoxia reduces the E-cadherin expression and increases OSCC cell migration regardless of the E-cadherin methylation profile. Pathol Res Pract 213, 496–501.

Fitzmaurice, C., Abate, D., Abbasi, N., Abbastabar, H., Abd-Allah, F., Abdel-Rahman, O., Abdelalim, A., Abdoli, A., Abdollahpour, I., Abdulle, A.S.M., Abebe, N.D., Abraha, H. N., Abu-Raddad, L.J., Abualhasan, A., Adedeji, I.A., Advani, S.M., Afarideh, M., Afshari, M., Aghaali, M., Agius, D., Agrawal, S., Ahmadi, A., Ahmadian, E., Ahmadpour, E., Ahmed, M.B., Akbari, M.E., Akinyemiju, T., Al-Aly, Z., AlAbdulKader, A.M., Alahdab, F., Alam, T., Alamene, G.M., Alemnew, B.T.T., Alene, K.A., Alinia, C., Alipour, V., Aljunid, S.M., Bakeshei, F.A., Almadi, M.A.H., Almasi-Hashiani, A., Alsharif, U., Alsowaidi, S., Alvis-Guzman, N., Amini, E., Amini, S., Amoako, Y.A., Anbari, Z., Anber, N.H., Andrei, C.L., Anjomshoa, M., Ansari, F., Ansariadi, A., Appiah, S.C.Y., Arab-Zozani, M., Arabloo, J., Arefi, Z., Aremu, O., Areri, H.A., Artaman, A., Asayesh, H., Asfaw, E.T., Ashagre, A.F., Assadi, R., Ataeinia, B., Atalay, H.T., Ataro, Z., Atique, S., Ausloos, M., Avila-Burgos, L., Avokpaho, E., Awasthi, A., Awoke, N., Ayala Quintanilla, B.P., Ayanore, M.A., Ayele, H.T., Babaee, E., Bacha, U., Badawi, A., Bagherzadeh, M., Bagli, E., Balakrishnan, S., Balouchi, A., Bärnighausen, T.W., Battista, R.J., Behzadifar, M., Behzadifar, M., Bekele, B.B., Belay, Y.B., Belayneh, Y.M., Berfield, K. K.S., Berhane, A., Bernabe, E., Beuran, M., Bhakta, N., Bhattacharyya, K., Biadgo, B., Bijani, A., Bin Sayeed, M.S., Birungi, C., Bisignano, C., et al., 2019. Global, Regional, and National Cancer Incidence, Mortality, Years of Life Lost, Years Lived With Disability, and Disability-Adjusted Life-Years for 29 Cancer Groups, 1990 to 2017: A Systematic Analysis for the Global Burden of Disease Study. JAMA Oncol 5, 1749–1768.

Fraga, C.A., de Oliveira, M.V., de Oliveira É, S., Barros, L.O., Santos, F.B., Gomez, R.S., De-Paula, A.M. and Guimarães, A.L., 2012. A high HIF-1α expression genotype is associated with poor prognosis of upper aerodigestive tract carcinoma patients. Oral Oncol 48, 130-5.

Gaonkar, R., Shiralgi, Y., Lakkappa, D.B., Hegde, G., 2018. Essential oil from Cymbopogon flexuosus as the potential inhibitor for HSP90. Toxicol Rep 5, 489–496.

Guimaraes, T.A., Farias, L.C., Fraga, C.A., Feltenberger, J.D., Melo, G.A., Coletta, R.D., Souza Santos, S.H., de Paula, A.M., Guimaraes, A.L., 2016. Evaluation of the antineoplastic activity of gallic acid in oral squamous cell carcinoma under hypoxic conditions. Anticancer Drugs 27, 407–416.

HaDuong, J.H., Blavier, L., Baniwal, S.K., Frenkel, B., Malvar, J., Punj, V., Sposto, R., DeClerck, Y.A., 2015. Interaction between bone marrow stromal cells and neuroblastoma cells leads to a VEGFA-mediated osteoblastogenesis. Int J Cancer 137, 797–809.

Hsu, S.S., Chou, C.T., Liao, W.C., Shieh, P., Kuo, D.H., Kuo, C.C., Jan, C.R., Liang, W.Z., 2016. The effect of gallic acid on cytotoxicity, Ca(2+) homeostasis and ROS production in DBTRG-05MG human glioblastoma cells and CTX TNA2 rat astrocytes. Chem Biol Interact 252, 61–73.

Keller, A., Nesvizhskii, A.I., Kolker, E., Aebersold, R., 2002. Empirical statistical model to estimate the accuracy of peptide identifications made by MS/MS and database search. Anal Chem 74, 5383–5392.

Lee, H.L., Lin, C.S., Kao, S.H., Chou, M.C., 2017. Gallic acid induces G1 phase arrest and apoptosis of triple-negative breast cancer cell MDA-MB-231 via p38 mitogen-activated protein kinase/p21/p27 axis. Anticancer Drugs 28, 1150–1156.

Liao, C.C., Chen, S.C., Huang, H.P., Wang, C.J., 2018. Gallic acid inhibits bladder cancer cell proliferation and migration via regulating fatty acid synthase (FAS). J Food Drug Anal 26, 620–627.

Locatelli, C., Filippin-Monteiro, F.B., Creczynski-Pasa, T.B., 2013. Alkyl esters of gallic acid as anticancer agents: a review. Eur J Med Chem 60, 233–239.

Ma, B., Zhang, K., Hendrie, C., Liang, C., Li, M., Doherty-Kirby, A., Lajoie, G., 2003. PEAKS: powerful software for peptide de novo sequencing by tandem mass spectrometry. Rapid Commun Mass Spectrom 17, 2337–2342.

McKenna, M.K., Gachuki, B.W., Alhakeem, S.S., Oben, K.N., Rangnekar, V.M., Gupta, R. C., Bondada, S., 2015. Anti-cancer activity of withaferin A in B-cell lymphoma. Cancer Biol Ther 16, 1088–1098.

Metri, R., Mohan, A., Nsengimana, J., Pozniak, J., Molina-Paris, C., Newton-Bishop, J., Bishop, D., Chandra, N., 2017. Identification of a gene signature for discriminating metastatic from primary melanoma using a molecular interaction network approach. Sci Rep 7, 17314.

Milanesi, S., Garibaldi, S., Saio, M., Ghigliotti, G., Picciotto, D., Ameri, P., Garibotto, G., Barisione, C., Verzola, D., 2019. Indoxyl Sulfate Induces Renal Fibroblast Activation through a Targetable Heat Shock Protein 90-Dependent Pathway. Oxid Med Cell Longev 2019, 2050183.

Monção, C.R.L., Santos, E.M., Prates, T.S., de Paula, A.M.B., Cardoso, C.M., Farias, L.C., Santos, S.H.S., D'Angelo, M.F.S.V., Guimarães, A.L.S., 2020. Immune/Neural approach to characterize salivary gland neoplasms (SGN). Applied Soft Computing 88, 105877.

Nesvizhskii, A.I., Keller, A., Kolker, E., Aebersold, R., 2003. A statistical model for identifying proteins by tandem mass spectrometry. Anal Chem 75, 4646–4658.

Nikishin, D.A., Filatov, M.A., Kiseleva, M.V., Bagaeva, T.S., Konduktorova, V.V., Khramova, Y.V., Malinova, I.V., Komarova, E.V., Semenova, M.L., 2018. Selection of stable expressed reference genes in native and vitrified/thawed human ovarian tissue for analysis by qRT-PCR and Western blot. J Assist Reprod Genet 35, 1851–1860.

Pang, Z., Zhou, G., Ewald, J., Chang, L., Hacariz, O., Basu, N., Xia, J., 2022. Using MetaboAnalyst 5.0 for LC-HRMS spectra processing, multi-omics integration and covariate adjustment of global metabolomics data. Nat Protoc 17, 1735–1761.

Park, W.H., 2017. Gallic acid induces HeLa cell death via increasing GSH depletion rather than ROS levels. Oncol Rep 37, 1277–1283.

Pereira, L.X., Alves da Silva, L.C., de Oliveira Feitosa, A., Santos Ferreira, R.J., Fernandes Duarte, A.K., da Conceição, V., de Sales Marques, C., Barros Ferreira Rodrigues, A.K., Del Vechio Koike, B., Cavalcante de Queiroz, A., Guimaraes, T.A., Freire de Souza, C. D. and Alberto de Carvalho Fraga, C., 2019. Correlation between renin-angiotensin system (RAS) related genes, type 2 diabetes, and cancer: Insights from metanalysis of transcriptomics data. Mol Cell Endocrinol 493, 110455.

Poswar, F.O., Fraga, C.A., Farias, L.C., Feltenberger, J.D., Cruz, V.P., Santos, S.H., Silveira, C.M., de Paula, A.M., Guimarães, A.L., 2013. Immunohistochemical analysis of TIMP-3 and MMP-9 in actinic keratosis, squamous cell carcinoma of the skin, and basal cell carcinoma. Pathol Res Pract 209, 705–709.

Qawoogha, S.S., Shahiwala, A., 2020. Identification of potential anticancer phytochemicals against colorectal cancer by structure-based docking studies. J Recept Signal Transduct Res 40, 67–76.

Rosenberg, A.R., Tabacchi, M., Ngo, K.H., Wallendorf, M., Rosman, I.S., Cornelius, L.A., Demehri, S., 2019. Skin cancer precursor immunotherapy for squamous cell carcinoma prevention. JCI. Insight 4.

Sánchez-Linares, I., Pérez-Sánchez, H., Cecilia, J.M., García, J.M., 2012. High-Throughput parallel blind Virtual Screening using BINDSURF. BMC Bioinformatics 13 (Suppl 14), S13.

Santos, E.M.S., da Rocha, R.G., Santos, H.O., Guimaraes, T.A., de Carvalho Fraga, C.A., da Silveira, L.H., Batista, P.R., de Oliveira, P.S.L., Melo, G.A., Santos, S.H., de Paula, A.M.B., Guimaraes, A.L.S., Farias, L.C., 2018. Gallic acid modulates phenotypic behavior and gene expression in oral squamous cell carcinoma cells by interfering with leptin pathway. Pathol Res Pract 214, 30–37.

Santos, E.M., Fraga, C.A.C., Xavier, A., Xavier, M.A.S., Souza, M.G., Jesus, S.F., Paula, A. M.B., Farias, L.C., Santos, S.H.S., Santos, T.G., Beraldo, F.H., Guimarães, A.L.S., 2021a. Prion protein is associated with a worse prognosis of head and neck squamous cell carcinoma. J Oral Pathol Med.

Santos, E.M., Fraga, C.A.C., Xavier, A., Xavier, M.A.S., Souza, M.G., Jesus, S.F., Paula, A. M.B., Farias, L.C., Santos, S.H.S., Santos, T.G., Beraldo, F.H., Guimarães, A.L.S., 2021b. Prion protein is associated with a worse prognosis of head and neck squamous cell carcinoma. J Oral Pathol Med 50, 985–994.

Schopf, F.H., Biebl, M.M., Buchner, J., 2017. The HSP90 chaperone machinery. Nat Rev Mol Cell Biol 18, 345–360.

Searle, B.C., 2010. Scaffold: a bioinformatic tool for validating MS/MS-based proteomic studies. Proteomics 10, 1265–1269.

Shalhout, S.Z., Emerick, K.S., Kaufman, H.L., Miller, D.M., 2021. Immunotherapy for Non-melanoma Skin Cancer. Curr Oncol Rep 23, 125.

Sourani, Z.M., Pourgheysari, B.P., Beshkar, P.M., Shirzad, H.P., Shirzad, M.M., 2016. Gallic Acid Inhibits Proliferation and Induces Apoptosis in Lymphoblastic Leukemia Cell Line (C121). Iran J Med Sci 41, 525–530.

Souza, L.R., Fonseca-Silva, T., Pereira, C.S., Santos, E.P., Lima, L.C., Carvalho, H.A., Gomez, R.S., Guimarães, A.L.S. and De Paula, A.M.B., 2011. Immunohistochemical analysis of p53, APE1, hMSH2 and ERCC1 proteins in actinic cheilitis and lip squamous cell carcinoma. 58, 352-360.

Souza, L.R., Fonseca-Silva, T., Santos, C.C., Oliveira, M.V., Corrêa-Oliveira, R., Guimarães, A.L., De Paula, A.M., 2010. Association of mast cell, eosinophil leucocyte and microvessel densities in actinic cheilitis and lip squamous cell carcinoma. Histopathology 57, 796–805.

Sun, C., Yuan, Q., Wu, D., Meng, X., Wang, B., 2017. Identification of core genes and outcome in gastric cancer using bioinformatics analysis. Oncotarget 8, 70271–70280.

Sung, H., Ferlay, J., Siegel, R.L., Laversanne, M., Soerjomataram, I., Jemal, A., Bray, F., 2021. Global Cancer Statistics 2020: GLOBOCAN Estimates of Incidence and Mortality Worldwide for 36 Cancers in 185 Countries. CA Cancer J Clin 71, 209–249.

Tabosa, A.T.L., Souza, M.G., de Jesus, S.F., Rocha, D.F., Queiroz, L., Santos, E.M., Guimaraes, V.H.D., Andrade, L.A.A., Santos, S.H., de Paula, A.M.B., de Souza, P.E.N., Farias, L.C., Guimaraes, A.L.S., 2022. Effect of low-level light therapy before radiotherapy in oral squamous cell carcinoma: An in vitro study. Lasers Med Sci.

Tiwari, R., Sahu, I., Soni, B.L., Sathe, G.J., Datta, K.K., Thapa, P., Sinha, S., Vadivel, C.K., Dhaka, B., Gowda, H., Vaidya, M.M., 2017. Quantitative phosphoproteomic analysis reveals system-wide signaling pathways regulated by site-specific phosphorylation of Keratin-8 in skin squamous cell carcinoma derived cell line. Proteomics 17.

Uhlen, M., Zhang, C., Lee, S., Sjöstedt, E., Fagerberg, L., Bidkhori, G., Benfeitas, R., Arif, M., Liu, Z., Edfors, F., Sanli, K., von Feilitzen, K., Oksvold, P., Lundberg, E., Hober, S., Nilsson, P., Mattsson, J., Schwenk, J.M., Brunnström, H., Glimelius, B., Sjöblom, T., Edqvist, P.H., Djureinovic, D., Micke, P., Lindskog, C., Mardinoglu, A., Ponten, F., 2017. A pathology atlas of the human cancer transcriptome. Science 357.

Wang, S., Tian, Y., Zhang, J.Y., Xu, H.B., Zhou, P., Wang, M., Lu, S.B., Luo, Y., Wang, M., Sun, G.B., Xu, X.D., Sun, X.B., 2018. Targets Fishing and Identification of Calenduloside E as Hsp90AB1: Design, Synthesis, and Evaluation of Clickable Activity-Based Probe. Front Pharmacol 9, 532.

Xavier, G.M., Guimarães, A.L.S., de Carvalho Fraga, C.A., Guimarães, T.A., de Souza, M. G., Jones, K.M., Farias, L.C., 2021. Pathways Related to the Anti-Cancer Effects of Metabolites Derived from Cerrado Biome Native Plants: An Update and Bioinformatics Analysis on Oral Squamous Cell Carcinoma. Protein Pept Lett 28, 735–749.

Zhou, J.W., Tang, J.J., Sun, W., Wang, H., 2019. PGK1 facilities cisplatin chemoresistance by triggering HSP90/ERK pathway mediated DNA repair and methylation in endometrial endometrioid adenocarcinoma. Mol Med 25, 11.